Multiple fragmentation mechanisms in ammonia: Collisions with protons in the intermediate velocity regime

W. Wolff [*], H. Luna,[†] and E. C. Montenegro[‡]
Instituto de Física, Universidade Federal do Rio de Janeiro, Rio de Janeiro, RJ, Brazil

L. C. Rodrigues Junior
Instituto de Física, Universidade Estadual do Rio de Janeiro, Rio de Janeiro, RJ, Brazil

The ionization and dissociation of ammonia by impact of protons is investigated experimentally in a wide range of energies from 125 to 2700 keV. Coincidence measurements are used to separate single from multiple ionization. The role of the charge sign of the projectile was analyzed for the ionization by comparing the proton with previous electron data. The energy dependence of the single and multiple-ionization cross sections allowed us to evaluate the role of second-order mechanisms. For single ionization, the role of a two-step mechanism was inferred. The double-ionization cross section showed that postcollisional deexcitation takes over the two-step sequential ionization above 800 keV. Triple ionization is prompted mostly by postcollisional Auger decay.

I. INTRODUCTION

Ammonia is common across the interstellar medium, as well as in proto-stars [1], in comets [2], in meteorites [3], and in the atmosphere and on surface of planetary bodies, e.g., Jupiter and Saturn's moon, Titan [4,5]. A large fraction of the nitrogen available for planet-forming regions, such as our early solar system, is believed to come from dissociated ammonia [6,7], which can be formed mostly by interaction with radiation, e.g., photons, electrons, and ions.

Besides, ammonia is the most common alkaline gas of the atmosphere, playing an important role in atmospheric chemistry and is closely related to the development of ecosystems, where ammonia is exposed to air. The CLOUD experiment at CERN [8] and the satellite data MIPAs [9] are examples which show that ammonia greatly increases the nucleation rate of atmospheric aerosols, which cause a cooling effect by reflecting sunlight and by seeding cloud droplets.

Also, in the biological and biomedical sciences, compounds containing nitrogen, such as ammonia, play an essential role in the evolution of terrestrial life [10]. When NH_3^{n+} dissociates, its fragments can combine with other molecules and molecular fragments in the vicinity, such as carbon and hydrogen radicals, and a number of new molecules and radicals can form, changing the environment. As discussed by Stein and Klotz [11], ammonia participates in the terrestrial nitrogen cycle, mainly in the fixation phase, where molecular nitrogen is removed from the atmosphere by microorganisms and transformed into ammonia, which will later be used for breeding of organic compounds spent in the metabolism of several living beings.

Understanding the interaction between energetic ions and ammonia molecules in the gaseous phase can provide important information on the mechanisms leading to dissociative ionization compared with single and double nondissociative ionization. This information is important for obtaining physical parameters in chemical models and astronomical observations [1,12].

In this work, we approach the ionization and subsequent dissociation of ammonia molecules in a gas phase induced by protons with energies varying from 125 to 2700 keV. In this intermediate-velocity regime, multiple ionization predominates over single ionization, while charge exchange, which prevails at lower velocities, is no longer important. In the experimental section we focus on extracting clean discriminated single- from multiple-ionization cross sections. This procedure allows us to uncover the processes present in the dissociative single and multiple ionization.

The measurements of cross sections, for proton impact, for single and multiple ionization channels have not yet been quantified in the literature, except for the fragmentation branching ratios leading to H_2^+ and H_3^+ formation at the energy of 4 MeV [13]. Other experimental results on proton impact, found in the literature, concern only the total ion production (total ionization) [14–16] and do not provide any information on the separation between n-fold ionization contributions in the fragment-ion production from dissociative ionization.

In order to extract information in the projectile sign effect on the ionization of ammonia, the present data were compared with electrons in the same velocity range of Refs. [17–21]. It is important to point out that ionization by electron impact, despite being extensively investigated, shows a large dispersion among the absolute cross sections reported.

[*]wania@if.ufrj.br
[†]hluna@if.ufrj.br
[‡]montenegro@if.ufrj.br

For the single-ionization analysis, we use a semi-empirical fragmentation matrix model based on the Born approximation [22–25] in order to extract the contribution from the single vacancy (vertical transitions) and from double-hole one-particle (2h-1p) satellite states. Here, valence orbitals are presented with some more detail as the fragment-ion formation depends on the orbitals of ammonia [26–28]. In this context the contributions from the valence molecular orbitals in the fragment-ion production are compared with those obtained by Wight *et al.* and Brion *et al.* [29,30] by electron emission $(e, 2e)$ and $(e, e + \text{ion})$ coincidence studies.

Concerning multiple ionization, we present the absolute experimental cross section (CS) for the long-lived dication NH_3^{2+}, and ion pairs. The present data show evidence of a postcollisional Auger decay contribution, from nitrogen K-shell ionization [31]. The competition between sequential ionization and postcollisional decay is discussed over the energy range studied in this work. The cross sections were also compared with those of double ionization induced by electron impact of Rejoub [21].

Finally, the net (sum over all channels) single, double, and triple ionization CSs were compared with the theoretical calculations based on the IAM-PCM model [32].

II. EXPERIMENT

Dissociative and nondissociative ionization cross sections were obtained using time-of-flight (TOF) mass spectroscopy combined with multicoincidence technique at the Atomic and Molecular Collision Laboratory of the Federal University of Rio de Janeiro, Brazil. The experimental setup consists of a proton beam with energies ranging from 125 up to 2700 keV, which crosses an ammonia effusive jet at right angles on the focus of the TOF mass spectrometer. After ionization, the ejected electrons and ionic fragments are extracted to opposite directions by a static electric field, being guided throughout the TOF. The electrons are focused and detected by an electron multiplier detector, while the ionic fragments are accelerated towards a field-free drift tube and further detected by a microchannel-plate detector. The proton beam was used at low currents to avoid secondary processes.

With a multihit coincidence setup, TOF spectra were obtained, setting the emitted electron(s) as the start pulse input and the ionic fragments of ammonia (recoil ions) as the sequential multihit STOP input signals. Therefore, one- and two-dimensional time spectra were obtained, simultaneously being related to single and multiple molecular ionization, respectively. To obtain from those spectra the true yields of fragment formation, the detection efficiencies need to be taken into account. The procedures are described in detail in previous and recent methane and water collision investigations [23,33]. A neon target was used to determine the ion and electron detection efficiencies by recoil-proton, electron-recoil, and electron-proton coincidence schemes throughout the ammonia experiments.

Concerning target preparation, the ammonia was purchased from Linde gas suppliers with a purity of 99.5%, liquefied to its own vapor pressure, and it was admitted into the interaction region via an effusive gas jet. The flow of ammonia was regulated by an ultrahigh leak valve which raised

the vacuum in the chamber from a base pressure of $\approx 8 \times 10^{-8}$ to 3.5×10^{-6} torr. Possible contamination of the system by critical impurities such as N_2 and H_2O was monitored. The injection line was heated before injection of ammonia and no water fragment ions were detected. A small amount of N_2^+ was detected. Therefore, the values of the known dissociative cross sections of N_2 [34] were used to determine the fraction of N_2^+ molecules that dissociate giving rise to a N^+ ion, and the contribution was accordingly subtracted.

The same experimental setup and procedures were applied to the proton-ammonia used in previous proton-methane and proton-water measurements [23,33]. The relative position of the gas jet in relation to the collimated projectile beam was adjusted to maximize their overlap in the focus of the time-of-flight spectrometer [35]. The ion, electron, and coincidence rates were monitored, the data sets were checked for reproducibility, and electron and ion detection efficiencies were measured via measurements for neon. The false coincidence events were minimized in the offline data reduction analysis [36] and the aliasing of coincidence events into lower-order events [37] were subtracted.

The true counts $N^t(Y^+)$ originated from NH_3^+ that dissociates into a neutral X and Y^+ ion ($NH_3^+ \rightarrow X + Y^+$) or into an ion pair X^+ and Y^+ ($NH_3^{2+} \rightarrow X^+ + Y^+$), can be obtained once the detection efficiencies involved in the measurement are determined. The electron detection efficiency ϵ was 0.25 and the fragment-ion detection efficiencies of H^+ and H_2^+, ρ_X, were from 0.14 to 0.17 and of N^+, N^{2+}, NH^+, NH_2^+, NH_3^+, and NH_3^{2+}, ρ_Y, from 0.21 to 0.26, respectively obtained along the time of measurement [23]. These efficiencies were obtained previously by normalizing the data of proton incidence on methane [23] to the data of Ref. [36] as a reference. We opted to apply the same efficiency correction procedure based also on the comparison of the kinetic energies of H^+ and H_2^+ measured for electron impact on methane and ammonia presented in Refs. [38–42]. They showed that the ionization of ammonia produces H^+ and H_2^+ fragments with even larger kinetic energies than in the methane ionization.

The equations which provide the true counts from the measured counts N^m are as follows:

$$N^t(NH_3^+) = \frac{N^m(NH_3^+)}{\rho_Y \epsilon}, \tag{1}$$

$$N^t(Y^+) = \frac{N^m(Y^+)}{\rho_Y \epsilon} - \frac{(1-\rho_X)}{\rho_X \rho_Y \epsilon} N^m(X^+, Y^+), \tag{2}$$

$$N^t(X^+) = \frac{N^m(X^+)}{\rho_X \epsilon} - \frac{(1-\rho_Y)}{\rho_X \rho_Y \epsilon} N^m(X^+, Y^+), \tag{3}$$

$$N^t(X^+, Y^+) = \frac{1}{\rho_X \rho_Y [1 - (1-\epsilon)^2]} N^m(X^+, Y^+), \tag{4}$$

where Y stands for N, NH, and NH_2 and X stands for H and H_2.

The true counts $N^t(NH_3^{2+})$ for the metastable double-ionized NH_3^{2+} and triple-ionized ion that dissociates into the ion pair N^{2+} and H^+ ($NH_3^{3+} \rightarrow N^{2+} + H^+$) are given by

$$N^t(NH_3^{2+}) = \frac{N^m(NH_3^{2+})}{\rho_Y [1 - (1-\epsilon)^2]}, \tag{5}$$

TABLE I. Absolute pure single-ionization and dissociation cross sections for ammonia at proton impact energies ranging from 125 to 2700 keV given in Mb. Uncertainties are found to be 7% for NH_3^+ and NH_2^+, 10% for NH^+ and H^+, 12% for N^+, and 18% for H_2^+.

E (keV)	N^+	NH^+	NH_2^+	NH_3^+	H^+	H_2^+
125	6.89	27.4	152.5	165.2	45.6	1.17
250	2.94	11.3	127.8	136.4	39.1	0.75
500	1.36	6.09	89.7	93.6	17.2	0.34
750	0.77	4.28	71.7	73.2	10.7	0.27
1000	0.62	3.57	57.5	58.7	7.44	0.19
1500	0.44	2.44	43.2	44.3	5.09	0.12
2000	0.36	2.01	34.5	35.3	4.31	0.11
2400	0.32	1.68	30.3	30.9	4.58	0.090
2700	0.24	1.44	28.2	28.7	2.99	0.073

and

$$N^t(N^{2+}, H^+) = \frac{1}{\rho_X \rho_Y [1 - (1 - \epsilon)^3]} N^m(N^{2+}, H^+). \quad (6)$$

Following this data reduction, the fragment ions that originate from a single (s) ionization event were separated from those resulting from the double (d) and triple (t) ionization events. After subtracting the false events, which come from the lack of sequential detection of one ion from an ion pair, we noted, for example, that at the proton impact velocity $v_p = 4.7$ a.u., counting all true NH^+ and N^+ ions irrespective of the degree of ionization, an enhancement of 21% and 44% relative to the true pure single counts, i.e., true $NH^+(s + d + t) = 1.21 \times$ true $NH^+(s)$ and true $N^+(s + d + t) = 1.44 \times$ true $N^+(s)$ is produced.

The absolute cross sections σ(ion, ion pair) were obtained by normalizing the true yield $Yield^t$ of pure single ions and parent dication (ion) and ion pairs (ion pair) to the suggested total ion production σ^+ cross sections of Rudd *et al.* [16]. In total, twelve channels were measured (see Tables I and II).

$$\sigma(\text{ion, ion pair}) = Yield^t(\text{ion, ion pair})\sigma^+, \quad (7)$$

where

$$Yield^t(\text{ion, ion pair}) = \frac{N^t(\text{ion, ion pair})}{\sum_{n=1}^{12} N_n^t(\text{ion, ion pair})}. \quad (8)$$

The recommended values by Rudd [16] were obtained through a fitting function over the energy range of 20 keV to 10 MeV. However, the fitting was based upon few measurements available on total ionization cross section: Those from Lynch *et al.* at the energies of 250, 1000, and 2000 keV [14] and by McNeal [15] at 20 and 30 keV. To evaluate Rudd's fitting, in particular in the energy region of the maxima of the total ionization CSs, we compare Rudd's fitting with the few recent theoretical results available in the literature in the range energy from 10 eV to 10 keV. Montanari [43] propose a neonization method treated with three different collisional formalisms: the continuum distorted-wave–eikonal initial state (CDW-EIS), the first order Born approximation (BA), and the shell-wise local plasma approximation (SLPA). Lüdde [44] calculated the net ionization cross sections based on the independent atom model (IAM) using the Bragg additivity rule and the so-called pixel-counting method (IAM-PCM) [49]. The geometric screening corrections introduced by PCM give substantially reduced cross sections for the net ionization cross sections and describe the proposed Rudd's cross sections well.

For electron impact, on the other hand, there are several experimental data and calculations of the total ionization cross section of ammonia reported in the literature, from threshold to high energies [31,46–48,50–53]. For comparison, the total electron ionization cross sections, two experimental [21,45]
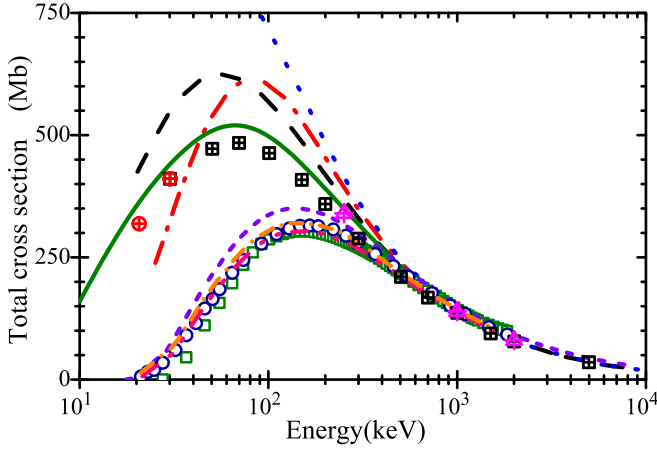
TABLE II. Absolute multiple-ionization cross sections for ammonia at proton impact energies ranging from 125 to 2700 keV given in Mb. Uncertainties are found to be 18% for (NH_3^{2+}), 15% for ($H^+ + NH_2^+$) and ($H^+ + NH^+$), 17% for ($H^+ + N^+$), and 30% for ($H^+ + N^{2+}$) and ($NH^+ + H_2^+$).

E (keV)	NH_3^{2+}	$H^+ + NH_2^+$	$H^+ + NH^+$	$H^+ + N^+$	$H^+ + N^{2+}$	$NH^+ + H_2^+$
125	0.27	12.1	7.91	3.92	0.063	0.10
250	0.11	3.52	2.37	1.14	0.019	0.027
500	0.047	1.39	0.87	0.42	0.013	0.016
750	0.035	0.88	0.50	0.28	0.012	0.014
1000	0.029	0.67	0.40	0.21	0.0089	0.0089
1500	0.022	0.59	0.31	0.17	0.0084	0.0077
2000	0.019	0.42	0.24	0.12	0.0081	
2400	0.017	0.31	0.18	0.10	0.0068	0.0042
2700	0.016	0.30	0.17	0.092	0.0065	0.0037

FIG. 1. Total ionization cross section: experimental proton data of Rudd (⊞) [16], McNeal (⊕) [15], and Lynch (✥) [14]; calculations of Montanari [43] SLPA (- - -), CDW-EIS (- . -) and BA (. . . .) and IAM-PCM (——) results of Lüdde [44]; experimental electron data of Rao (□) [45] and Rejoub (○) [21]; and BEB calculations of Hamilton (- - -) [46], Kim (. . . . .) [47], and Hwang (. . . . .) [48].

FIG. 2. Ratios of NH_2^+ fragment-ion yield with respect to NH_3^+ under proton impact (connected by line to guide the eye): present work single (–■–) and total (★); under electron impact from the literature indicated by first author Rejoub (●) [21], Bederski (◆) [18], Rao (▲) [45], Syage (▼) [54], Märk (◄) [19], Crowe (►) [20], and Tarnovsky (⬟) [55] and electron-impact calculations Khare (- . -) [51], Saksena (- . . .) [52], and Hamilton (- . . .) [46].

and three calculations based on the binary-encounter-Bethe model (BEB) [46–48] are also shown in Fig. 1.

III. RESULTS AND DISCUSSION

A. Experimental cross sections

The cross sections of ionic fragment production for single, double, and triple ionization of ammonia molecule in a gas phase are listed in Tables I and II. The uncertainty in the cross sections presented here comes from the standard error derived from the averaging process in multiple sets of measurements, detection efficiencies, and the normalization data procedure.

B. Fragment-ion ratios with respect to the parent ion

In Figs. 2–4 we compare the ratio between cross sections of the fragment-ions NH_2^+, NH^+, and N^+ in relation to the parent ion NH_3^+ measured in the present work under proton impact $R_p(Ion)$ to equivelocity electron data obtained from the literature $R_e(Ion)$ of Refs. [18–21,45,54]. The ratios $R_p(Ion)$ are defined as the ratios of the fragment-ion true events divided by the true parent-ion intensity as follows: $R_p(Ion) = N^t(Ion)/N^t(NH_3^+)$. In these figures we present the ratios of the fragment-ions formed only by pure single ionization (black solid squares) as well as those that account for the fragment-ions produced by single, double, and triple ionization, indicated as total in the figure caption (gray closed stars). In the Figs. 2–4, the *y*-axis title indicates that both $R_p(Ion)$ and $R_e(Ion)$ are shown.

It should be noted that most of the electron-impact data, except for the work of Rejoub and coworkers [21], which collected also the ion pairs, do not separate single, double, and triple ionization. Their measurements account for the total ion-formation channels without taking into account any correction of false coincidences (due to the lack of detection
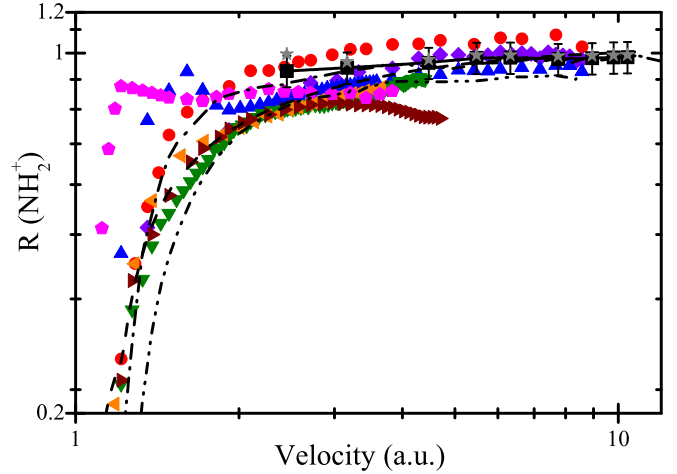
of at least one ion from the ion-pair fragments), as discussed in the experimental section of this work.

From Figs. 2–4 we can also observe that, except for the NH_2^+/NH_3^+ ratio, there is poor agreement among the electron data available in the literature. Towards low velocities, as expected, the electron data fall due to the ion formation thresholds while the ratios obtained under proton impact increase. For instance, for proton impact, this behavior shows that, toward lower velocities, the fragments NH^+ and N^+ have a different velocity dependence than NH_2^+ and NH_3^+ fragments.

For the ratio of NH_2^+ (Fig. 2) there is good agreement between the ratios measured under proton impact and those obtained under electron impact, considering the relatively low dispersion of the data and experimental uncertainties. The ratios $R_p(NH_2^+)$ as well as $R_e(NH_2^+)$ have a flat behavior above velocities of 3 a.u., indicating that NH_2^+ and NH_3^+ production have the same velocity dependence for proton and electron impact. The theoretical electron-impact calculations [46,51,52], included in the figure, are in agreement with this result.

However, for $R_e(NH^+)$ and $R_e(N^+)$ [see Figs. 3(a) and 3(b)], discrepancies among the electron data become significant. Despite that overall discrepancy, there is a general trend showing that the ratios $R_e(NH^+)$ and $R_e(N^+)$ obtained under electron impact from the literature are larger [18,20,21,54] or approximately equal [45] to the ratio $R_p(NH^+)$ and $R_p(N^+)$ measured under proton impact except for the one data set of Märk [19].

For hydrogen ionic fragments, H^+ [Fig. 4(a)] and H_2^+ [Fig. 4(b)], there are also discrepancies among the existing electron data. Except for one data set [21], all other H_2^+ ratios are lower than the measured ones for proton impact. H^+ are produced with larger kinetic energies than the NH_n^+ ions as result of the kinematics of momentum transfer [21,40,41,54,56].
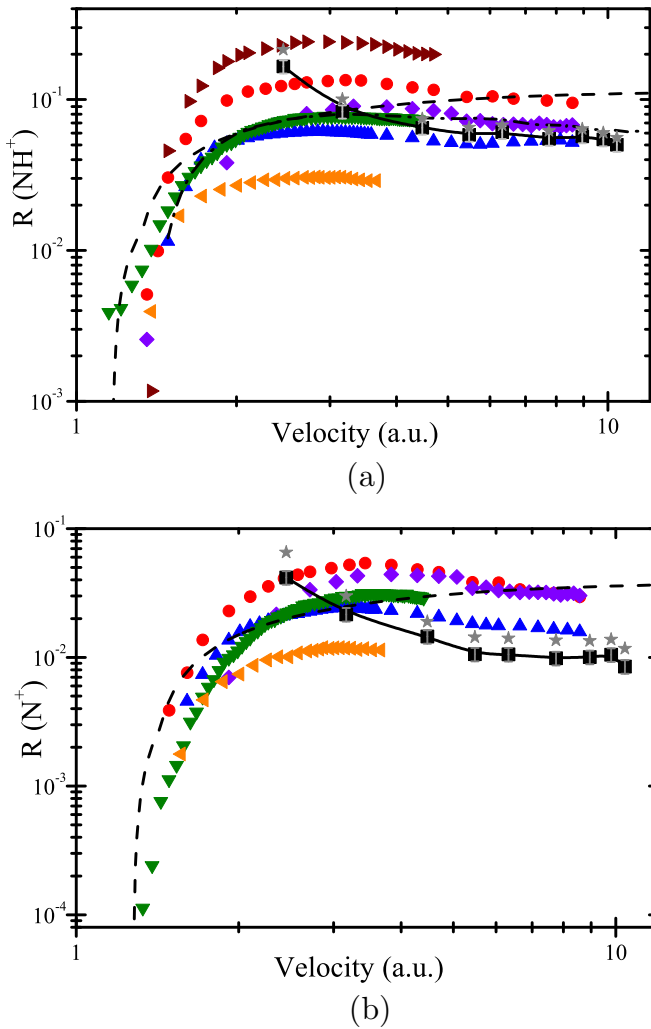
FIG. 3. Ratios of NH^+ (a) and N^+ (b) fragment-ion yields with respect to NH_3^+ under proton impact (connected by line to guide the eye): present work single (—■—) and total (★); under electron impact from the literature indicated by first author Rejoub (●) [21], Bederski (◆) [18], Rao (▲) [45], Syage (▼) [54], Märk (◀) [19], Crowe (▶) [20] and electron-impact calculations Hamilton (▪▪▪▪) [46].

FIG. 4. Ratios of H^+ (a) and H_2^+ (b) fragment-ion yields with respect to NH_3^+ under proton impact (connected by line to guide the eye): present work single (—■—) and total (★); under electron impact from the literature indicated by first author Rejoub (●) [21], Bederski (◆) [18], Rao (▲) [45], Syage (▼) [54], Märk (◀) [19].

Comparison between R_e(Ion) and R_p(ion) (at the same velocities) can shed light into the influence of the projectile charge sign in the ionization of molecules, and in the subsequent ion fragment formation [34]. For methane [23], on the contrary to that found in helium [57–59], the difference in the ionization cross section due to the projectile charge sign are found to be significant only in the single ionization, in particular, in the channel with higher degree of fragmentation. For ammonia, the present data combined with the existing electron-impact data cannot provide a clear statement of the projectile sign effect in the single ionization due to the large dispersion of the electron data. However, by comparing Figs. 2 and 3 one can note a trend similar to that observed for methane, i.e., of N^+ having a smaller ratio for protons than for electrons. Projectile charge effects in single ionization of molecular targets were reported by antiproton and proton impact [60,61] and positron and electron impact [62].
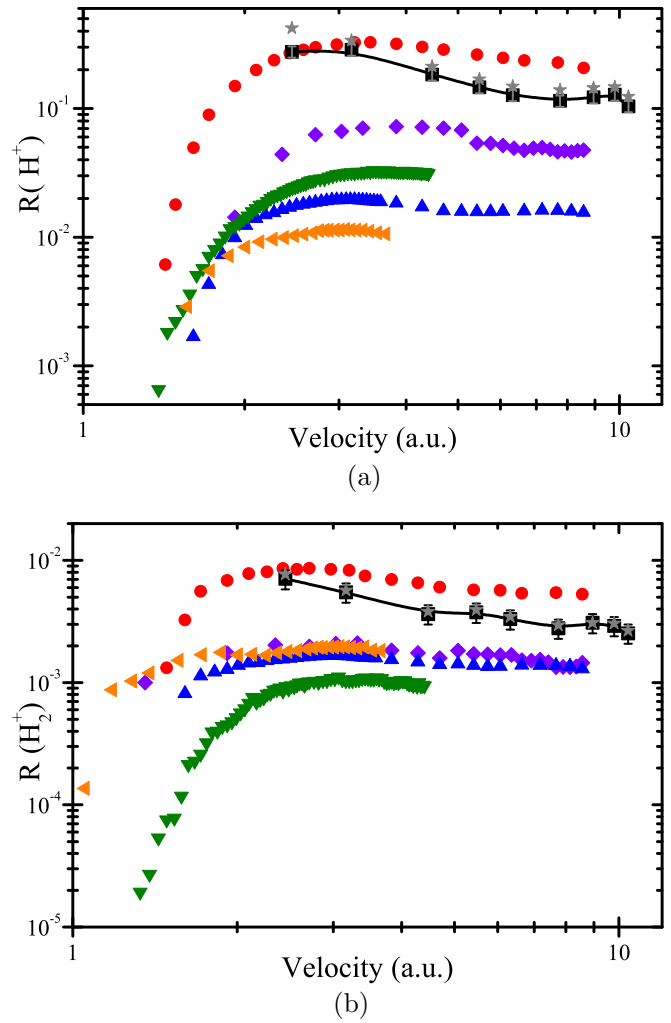
Satellite states can be populated in the single-ionization process by either shake-up or by a two-step type mechanism when the projectile interacts with two electrons, ejecting one and exciting the other. In the case of ammonia there are several satellite bands assignable to transitions leading to dissociation from an excited ionic state prepared by the shake-up transition or from a doubly excited state converging to an excited ionic state. These mechanisms are indistinguishable when leading to the same final states, and they give rise to an interference in the probability amplitudes leading to interference terms which are proportional to Z_p^3, where Z_p is the projectile charge [63]. The interference term is positive for electrons and negative for protons [23].

C. Single ionization

The scenario suggested in the previous section can be better evaluated with the aid of the semi-empirical fragmentation matrix model (FMM), an approach used successfully for small

molecules, such as water, methane, and DNA base analogs [23–25,33]. This approach correlates the cross sections for the single valence vacancies to the measured fragment-ion single-ionization cross sections. The ionization potential of the molecular orbitals, the appearences energies of the fragmentions, and the breaking curves are available in the literature. They provide the baseline for the assignment of the fragmentation factors associated with each orbital state [22,24].

To choose these constants properly it is necessary to take into account the electronic configuration of ammonia, which is described here briefly. The Hartree-Fock electronic configuration of ammonia is in C_{3v} symmetry $(1 a_1)^2$, inner shell, $(2 a_1)^2$, inner valence, and $(1 e_1)^4$ and $(3 a_1)^2$, outer valences. The 3 a_1 and 1 e_1 outermost orbitals are considered both to have p-like character. In contrast, the 2 a_1 orbital is viewed as an s-type orbital [64,65]. The 3 a^{-1} and 1 e^{-1} states are pure single-hole states while the 2 a^{-1} state involves configurations other than a 1h state. It consists of a strong configuration mixing between the single-hole 2 a^{-1} state and predominantly 2h-1p states (satellite states) [26–28].

The single hole states were determined at 10.85 and 16.4 eV by high-momentum-resolution electron momentum spectroscopy and electron-energy-loss spectrum of NH_3 tagged with fluorescence photons and calculated by using the symmetry-adapted-cluster configuration-interaction general-R method and a configuration-interaction calculation at 10.57 eV (10.94 eV), and 16.46 eV (16.50 eV) [26–28]. In contrast, the 2 a^{-1} state is composed by a manifold of final ion states due to many-body effects and five satellite bands can be assigned [27]. The first band is composed of three states, with a main peak at 27.6 eV [28], which involve excitation to valence antibonding orbitals calculated at 26.76 and 28.79 eV and those to Rydberg orbitals at 27.98 eV. EMS measurements show, for ammonia as well as methane, that the next satellite bands show a small spectral intensity $\approx 10\%$ of the band 1 [27,28,65]. The second band states are observed at 30.3 eV and calculated at 29.76 and 29.81 eV. The third band is composed by eleven states calculated from 30.75 to 35.05 eV and measured clustered around 33.2 eV. Bands 4 and 5, which lay above the double-ionization threshold (33.76 eV) were observed around 36.5 and 41.8 eV [66]. Therefore, it is noticeable that, in the energy range of the inner-valence orbitals, the density of 2-hole 1-particle (2h-1p) configurations is high and can no longer be expected to correspond to a single-hole configuration [65].

For the case of ammonia, the outer and inner-valence ionization energies ($I_P = I_{MO}$) of ionized NH_3 extends up to 42 eV through several satellite states. The first two bands of 2 a^{-1} with monopole intensities of 1.00 and 0.16 [27] were taken into account in the model with $I_P = 27.3$ and 30.3 eV with relative contribution weights of 1 and 0.16. We excluded the higher band structures because they are more likely to lead to dissociative double-ionization channels [40].

Besides the relevance of the molecular states in the model, the threshold energies for dissociation and breakdown curves of the fragment-ion production need to be taken into account in the model calculations. To ensure these conditions, the fragment-ion appearance energies (E_{app}) and ionization efficiency curves measured by electron impact [19,29,30,40,41,56,67,68] were taken as references. The frag-
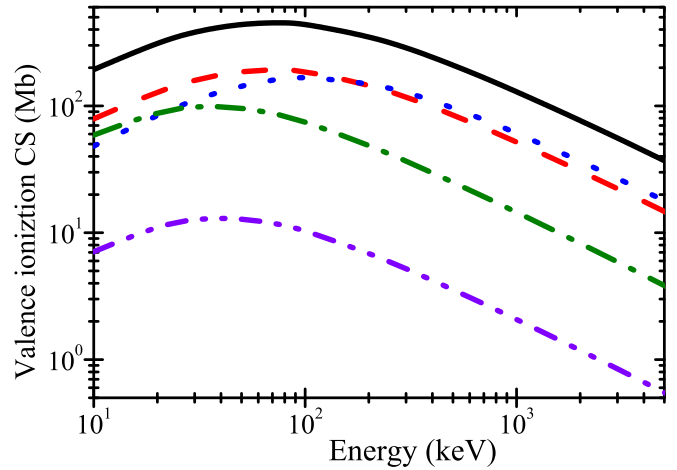

FIG. 5. Single-ionization cross sections of outer valence 3 a^{-1} (- - -) and 1 e^{-1} (. . .) and inner 2 a^{-1} band 1 (——) and band 2 (- - - - -) and sum (——) of the 3 a^{-1}, 1 e^{-1}, 2 a^{-1} band 1 and 2 states (total FMM) in Mb.

ment ions are produced starting at the appearance energy onsets through dissociative ionization and predissociation (14.7–19.5 eV) dissociative autoionization (Rydberg excitation), dissociative ionization (24.5–30 eV), and dissociation through a cascade of processes [29,30,40,68].

As the semi-empirical fragmentation matrix model is applicable only to single ionization, we discarded the appearance energy onsets of the highly energetic ions which are associated with double and triple ionization. We considered as our baseline the following values for the appearance energies (E_{app}) of the fragments: $E_{app}(NH_3^+) \approx 11$ eV, $E_{app}(NH_2^+) \approx 17$ eV, $E_{app}(NH^+) \approx 23$ eV, $E_{app}(N^+) \approx 28$, eV, $E_{app}(H^+) \approx 22$ eV, and $E_{app}(H_2^+) \approx 24$ eV.

The fragmentation matrix model was detailed previously [22,24,25], so only an outline of the model is given here. The fragmentation fractions (matrix elements) are selected considering a set of criteria, which includes the appearance energies of the fragment-ion. The correlated analysis of the molecular orbital (MO) ionization potentials and the appearance energies of the fragments allows us to select the MOs which are energetically eligible and may induce the particular fragment ion. Additional criteria include the condition that the calculated cross section should reproduce the experimental cross section at high energies. Therefore, in the process of filling the matrix, it is important to compare the shape of the calculated cross section as functions of the energy with the measured one [24,25,69]. The functional equation [Eq. (9)] describes well the behavior at high energies as it is based on the Born approximation, becoming less accurate at lower energies. The valence orbital ionization cross sections shown in Fig. 5 were calculated by using the scaling suggested in Ref. [22]:

$$\frac{\sigma_{MO} I_{MO}^2}{Z_{MO} \delta_{MO}} = \frac{A \ln (1 + Bx)}{x} - \frac{AB}{(1 + Cx)^4}, \quad (9)$$

with two sets of adjustable parameters (A, B, and C), $A = 8200$, $B = 0.035$, $C = 0.0075$, for the outer valence orbitals and $A = 4400$, $B = 0.30$, $C = 0.0041$ for the inner

TABLE III. (a) Fragmentation matrix, proton impact, and (b) $(e, e + \text{ion})$ data, electron loss. 3 a^{-1} and 1 e^{-1} are single hole states and the 2 a^{-1} state consists of a manifold of satellite bands. The numbers in parentheses denote band one or band two. The last column in the proton matrix is the sum of the matrix elements of 2 a^{-1} satellite bands.

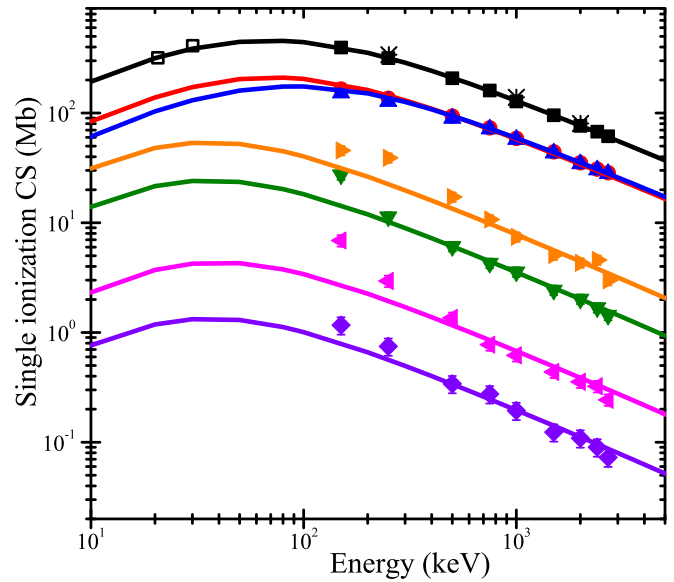|			(a) Proton		
Ions	$3a^{-1}$	$1e^{-1}$	$2a^{-1}(1)$	$2a^{-1}(2)$	$2a^{-1}(1+2)$
NH_3^+	1	0.10			
NH_2^+		0.90	0.3		0.3
NH^+			0.2	0.05	0.25
N^+				0.05	0.05
H^+			0.49	0.055	0.55
H_2^+			0.01	0.004	0.014
			(b) Electron		
Ions	$3a^{-1}$	$1e^{-1}$	$2a^{-1}$		
NH_3^+	1	0.20			
NH_2^+		0.80			
NH^+			0.34		
N^+			0.07		
H^+			0.59		
H_2^+					

FIG. 6. Experimental pure single-ionization cross sections and calculations based on the semi-empirical fragmentation matrix model (FMM) in Mb. Present work: experiment (symbols) NH_3^+ (●), NH_2^+, (▲) NH^+ (▼), N^+ (◄), H^+ (▷), H_2^+ (◆), and previous experimental work on total CS Rudd [16] (■), McNeal (□) [15], Lynch (✳) [14], and fragmentation matrix model (solid lines) (FMM), NH_3^+ (——), NH_2^+ (——), NH^+ (——), N^+ (——), H^+ (——), H_2^+ (——), and total CS (——).

valence orbital bands. The parameters $x = (E/M)/I_{MO}$, and E/M (impact proton energy/mass) in keV/amu and the I_{MO}, the ionization energies ($I_P = I_{MO}$), in units of Rydberg ($I_{MO}/13.6$ eV), gives σ_{MO} in Mb. The label MO represents a particular molecular orbital. Z_{MO} is the number of electrons in each state, two for 3 a^{-1}, four for 1 e^{-1}, and two for 2 a^{-1} band 1 and band 2 with relative intensities of 1 and 0.16, and δ_{MO} is taken as 0.5 in all cases.

The calculated cross sections for single ionization are plotted in Fig. 5. The calculated total ionization cross section (total FMM) is obtained by summation of the cross sections of single hole and satellite states(3 a^{-1} + 1 e^{-1} + 2 a^{-1}, band 1 plus band 2). The individual cross sections were distributed according to a matrix defined by a set of fragmentation fractions [24,25,69] and listed in Table III(a) among the ammonia cations. The matrix elements are not unique and some freedom to change the tabulated values exists.

The cross sections indicated as solid lines for the cations NH_n^+ and H_m^+ were obtained by the product of the fragmentation fractions and the ionization cross section of the molecular orbital where a single vacancy is produced. The experimental cross sections, shown by symbols, displayed in Fig. 6, account accordingly only for those ionization or dissociative breakup cross sections, where the parent ion is formed or dissociates via a single charged fragment plus one or more hydrogen atoms or neutral radicals ($NH_3^+ \rightarrow NH_2^+ + H$, $NH^+ + 2H$ or H_2, $N^+ + 3H$, $H^+ + NH_2$, $H_2^+ + NH$).

The good agreement between the experimental and FMM cross sections shown in Fig. 6 demonstrates that the semi-empirical FMM approach provides a reliable tool to estimate the contribution of the valence shell single ionization in the fragment-ion of NH_3^+ and NH_2^+ production over the entire measured energy range and of all other fragment ions above 250 keV.

The semi-empirical model does not fit properly the single-ionization channels leading to NH^+, N^+, H^+, and H_2^+ for energies below 400 keV. This is an indication that, at these lower energies, process(es) with a different single electron vacancy energy dependence [Eq. (9)] must be taken into account. Mechanisms with different energy dependencies than the one associated with the production of a single vacancy must be considered.

Satellite 2h-1p states can be populated either by shake-up following the production of a single vacancy in the 2 a_1 orbital or via two consecutive projectile interactions, ionizing one electron and exciting another, referred to in the literature as two-step-two (TS2) [57]. The first mechanism is included in the fragmentation matrix model displayed in Fig. 6. The cross section for the latter has the same energy dependence than a sequential two-step double-ionization cross section, which in a perturbative approximation scales with the projectile kinetic energy as $1/E^2$ and is not included in the fragmentation matrix model. We suggest that the deviation seen in Fig. 6 between the fragmentation matrix model results and the experimental data for the NH^+, N^+, H^+, and H_2^+ channels reflects the fact that the fragmentation matrix model does not take into consideration the TS2 mechanism to feed the 2h-1p satellite states for intermediate velocities. For higher velocities, the TS2 mechanism loses importance.

Correlating fragmentation spectra of single ionized ions to a MO state model was also pursued by Brion *et al.* and Wight *et al.* [29,30] in electron-impact experiments. In their works, the partition factors obtained by the dipole breakdown picture (DBP) are listed in Table III(b) [29,30]. In the DBP, the
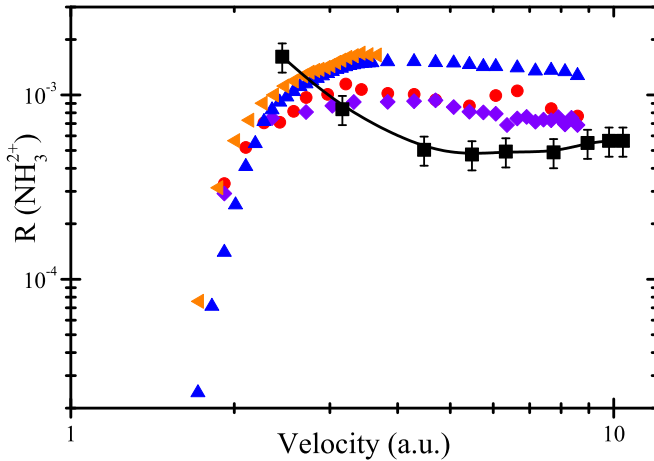
FIG. 7. Ratio of the double-ionized ammonia ion NH_3^{2+} yield with respect to NH_3^+ under present proton impact (connected by lines to guide the eye): single (–■–); for experimental electron impact from the literature indicated by first author Rejoub (●) [21], Bederski (◆) [18], Rao (▲) [45], and Märk (◀) [19].

FIG. 8. Ion-pair double-ionization cross sections for proton collision indicated by full symbols (NH_2^+, H^+) (–■–), (NH^+, H^+) (–■–), (N^+, H^+) (–■–), and (NH^+, H_2^+) (–■–), and for electron impact [21] by open symbols, (ND^+, D^+) (○) and (N^+, D^+) (□) in Mb. Symbols are connected by lines to guide the eye.

fragmentation picture was built with the aid of the branching ratios for the three states of ionized NH_3 and the partial oscillator strengths for formation of the electronic states of NH_3^+ [29,30].

The present work on proton collision as well as the $(e, 2e)$ plus $(e, e + \text{ion})$ energy-loss experiment [29] suggest the following assignments: the 3 a_1 state leads only to NH_3^+ formation; the 1 e_1 state produces the remaining NH_3^+ and NH_2^+; the 2 a_1 states forms H^+, N^+, H^+, and H_2^+ ions and still some NH_2^+. The FFM suggests that the 2 a_1 state also gives rise to NH_2^+, which is not foreseen by DBP. The FFM makes a distinction from which band of the manifold of the 2 a_1 states, first and/or second satellites bands [indicated in Table III(a) by 2 a_1(1) and 2 a_1(2)] the NH^+, N^+, H^+, and H_2^+ fragments are produced. Both simplified pictures evidently give the main features of the ammonia ion formation, and agree well with each other, as shown in Table III.

D. Double ionization

The double ionization of ammonia leads to both the nondissociative NH_3^{2+} dication and the dissociative ion pairs (e.g., $H^+ + NH_2^+$, $H^+ + NH^+ + H$, $H^+ + N^+ + 2H$, and $H_2^+ + NH^+$). The threshold energy obtained from electron-impact experiments for the doubly ionized states of NH_3 occurs at the energy of 34 eV where the dication starts to be produced [19,66,67]. According to Appel [70], the NH_3^{2+} dication can be long-lived with a lifetime $\geqslant 10$ μs. It can also dissociate more slowly or rapidly [71], depending on their geometry and/or internal energy electronic states.

We measured stable NH_3^{2+} states with lifetime of $\geqslant 10$ μs [19,66]. In Fig. 7 ratios of NH_3^{2+}/NH_3^+ are compared with the electron-impact data [18,19,21,45]. Above $v = 3.0$ a.u., all electron-impact yields are larger in magnitude than the proton yields, but both ratios show a plateau-type structure at high velocities. This finding will be further discussed below.
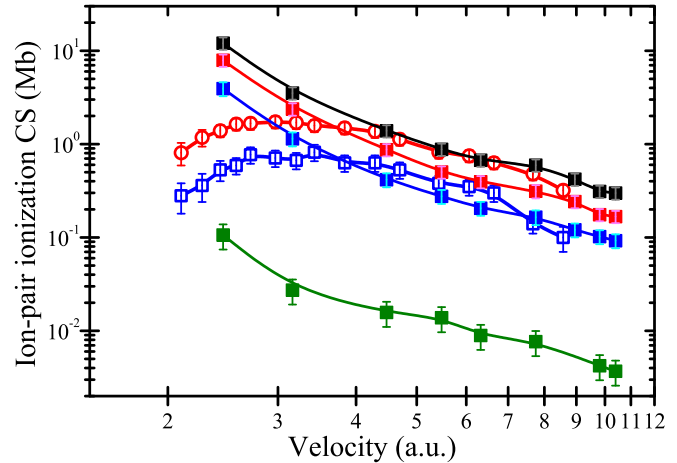
The dissociative double-ionization channels of NH_3^{2+} were reported in detail in Refs. [40,72] for electron impact, leading to the formation of several ion pairs:

1. $H^+ + NH_n^+$, with $n = 0, 1,$ and 2;
2. $H_2^+ + NH_n^+$, with $n = 0$ and 1;
3. $H^+ + H^+ +$ neutral(s).

They found out that the onset energies for the production of the ion pairs (NH_2^+, H^+), (NH^+, H) and (N^+, H^+) depend strongly on the decomposition of the doubly ionized NH_3^{2+} states at 34.9, 37, 39.5, and 44.5 eV. Appearance energies of H^+ at 34.9, 36.2, 39.2, and 45.7 eV were mainly ascribed to NH_3^{2+} dissociation channels, while for H_2^+ the thresholds were measured at 35.6 and 46.4 eV. The dissociation channel, lowest in energy, leading to H_2^+ is through NH^+ production [40,41,56,71,72].

The cross sections for the third case were not measured because the present experimental setup was not able to distinguish between the two H^+ arriving almost simultaneously at the detector, interpreting this as a single stop signal. This channel is then wrongly counted as a single hit and therefore as a single-ionization event. The effect of it in the net single ionization can be disregarded due to the orders of magnitude difference between the cross sections. For methane, the channel $H^+ + H^+ +$ neutral(s) plays a minor role on the net double ionization [23,36], therefore we assume that this channel makes a minor contribution to the net double ionization.

Absolute partial cross sections for production of the ion pairs (NH_2^+, H^+), (NH^+, H^+), (N^+, H^+), and (NH^+, H_2^+) are shown in Fig. 8 and present the following cross-section relation: $\sigma(NH_2^+, H^+) > \sigma(NH^+, H^+) > \sigma(NH^+, H^+)$. We added to the figure the dissociation cross section of the ion pairs (ND^+, D^+) (N^+, D^+) measured for electron energies from threshold to 1000 eV by Rejoub *et al.* [21]. It should be noted that the dissociation into the $ND_2^+ + D^+$ pair was not reported in this work [21]. A good agreement, in absolute values, between proton and electron data was found for velocities above $v = 3$ a.u., as shown in Fig. 8. At higher velocities
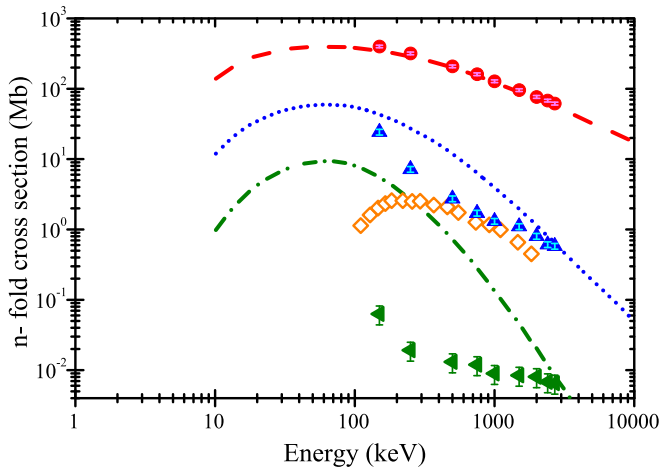
FIG. 9. Total single- and multiple-ionization cross sections in Mb. The present experimental data for proton single ionization (SI, ●), double ionization (DI, ▲), and triple ionization (TrI, ◀); IAM-PCM calculations for protons [44], SI (– – –), DI (. . . .), and TrI (——); and the electron data of Rejoub (◇) [21].

the multiple ionization by electron and proton impact coalesce because these cross sections are dominated by postcollisional processes (Auger-like processes). This trend was observed in noble gases [73] as well as in water and methane [23,33]. At low energy the electron cross sections fall due to the closing of the multiple-ionization channels, while proton cross sections still increase and are expected to reach the maximum at around 80 keV (see Fig. 9).

Physical processes behind double ionization can be separated between two distinct interaction mechanisms. In one mechanism the projectile interacts and ionizes sequentially two electrons of the target, which is known as a double-vacancy mechanism. In the other, the projectile interacts and ionizes one electron from an inner shell (nitrogen K shell for ammonia) as a single-vacancy mechanism, and the second electron is autoionized as postcollisional effect (Auger-like decay). It is important to note that, based on arguments of the first-order theories, we would expect these competing mechanisms to have different energy dependencies ($\approx 1/E^2$ for the double vacancy and $\approx 1/E$ for the single vacancy). A function $C/E + D\sigma(K\text{-shell})/\sigma(\mathrm{NH_3^+})$ was used to fit the double-ionization ratios (see Fig. 10), taking into account these one-step [$D\sigma(K\text{-shell})/\sigma(\mathrm{NH_3^+})$] and two-step ($C/E$) mechanisms (see Fig. 10). The first term corresponds to the dependence of the ratio between a double and a single-vacancy production, and the second term represents the contribution from the ratio of the K-shell cross section to the $\mathrm{NH_3^+}$ cross section. To separate both contributions, the ratio between the nondissociative and dissociative double-ionization and the parent ion cross sections were analyzed, as function of the impact energy E as shown in Fig. 10.

In the case of ammonia, we considered as K-shell cross sections that of the nitrogen atom calculated using the software ISICS based on plane-wave Born approximation (PWBA) and energy loss (E), Coulomb deflection (C), perturbed stationary state (PSS), and relativistic (R) effects (ECPSSR) theory [74]. The constants C and D are free param-
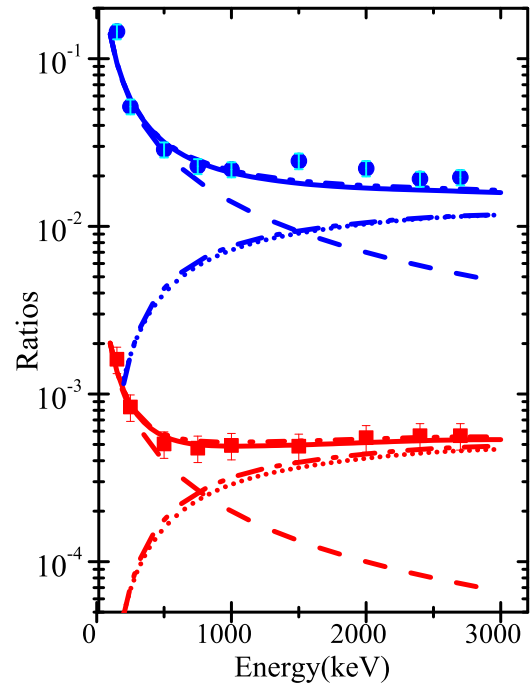

FIG. 10. Ratio of nondissociative double-ionization (non-dis DI) ($\mathrm{NH_3^{2+}}$) (■) and dissociative double ionization (dis DI) (sum of ion pairs, ●) to pure single $\mathrm{NH_3^+}$ ionization cross sections for proton collision; experimental data indicated as symbols and functions as lines, blue color indicates dis DI and red indicates non-dis DI. C/E (– – –), $D\sigma(K\text{-shell})^{\mathrm{PWBA}}/\sigma(\mathrm{N_3^+})$ (. . . . . .), $D\sigma(K\text{-shell})^{\mathrm{ECPSSR}}/\sigma(\mathrm{N_3^+})$ (———), sum of the two function terms with PWBA (———) and ECPSSR (———).

eters and were adjusted individually to the ratios of nondissociative and dissociative double ionization ($C_{\text{non-dis-DI}} = 0.2$, $C_{\text{dis-DI}} = 14$, $D_{\text{non-dis-DI}} = 0.04$, and $D_{\text{dis-DI}} = 0.96$). It can be seen from Fig. 10 that the contributions from sequential double ionization (TS2) and postcollisional double ionization (Auger decay) play their role differently along the entire energy range. Figure 10 depicts an additional feature: for the dication production, the postcollisional decay takes over the TS2 process at an impact energy ≈ 800 keV, while TS2 still dominates the dication breakup up to ≈ 1500 keV.

E. Multiple ionization

Figure 11 displays the ratio of cross sections for multiple-ionization channels with respect to the parent ion ($\mathrm{NH_3^+}$). The single ionization dominates the ionization scenario—there is a marked competition between the dissociative and nondissociative ionization, but the dissociation process prevails slightly and increases at lower energies. In contrast, in the double ionization the dissociative process leading to ion-pair formation strongly prevails over the long-lived doubly charged parent ion production. For both processes, at lower proton collision energies, a much larger enhancement is observed in comparison with the single ionization. The triple ionization is very weak and the constant ratios demonstrate that the Auger deexcitation process dominates almost over the entire energy range.
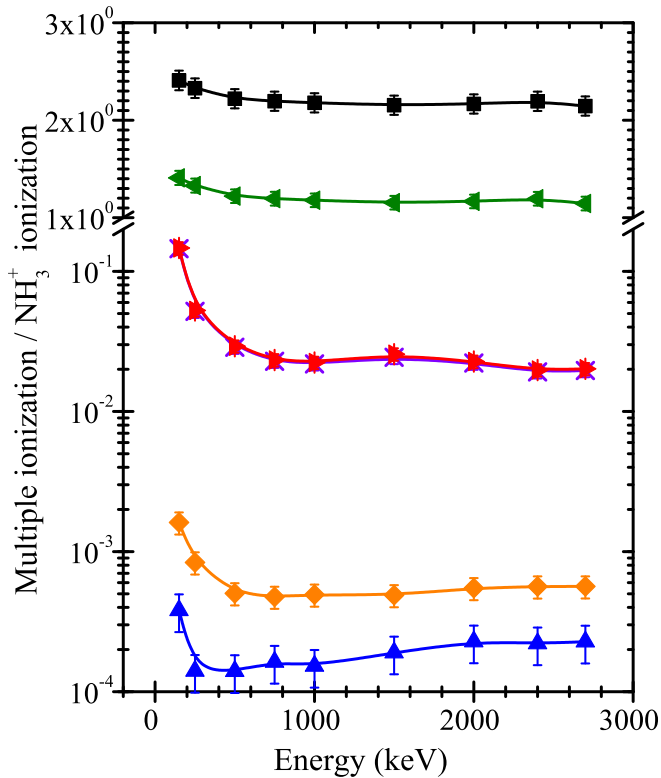
FIG. 11. Ratio of cross sections for multiple-ionization channels relative to the parent ion, where SI (■), DI (▶), and TrI (▲), designate single, double, and triple ionization, respectively, and Dis SI, dissociative single ionization (◀), non-Dis DI (◆), and Dis DI, dissociative double ionization (✖).

A comparison with the theory is shown in Fig. 9. While the IAM-PCM [44] results agree quite well with the measured experimental single- and total-ionization cross sections (see Fig. 1), the double and triple ionization show very little agreement between experimental data and theory, in particular, in the energy dependence. For comparison, we added to Fig. 9 the sum of the two ion pairs and metastable dication cross sections for electrons [21]. Note that the electron energies were converted to equivalent proton energies. Once again, below the cross section maxima of the electron data, the difference to the proton cross sections is continuously enhanced with decreasing impact energy, but above ≈400 keV, both absolute values tend to coalesce.

IV. SUMMARY AND CONCLUSIONS

A systematic investigation of single and multiple ionization of ammonia by protons was presented in a range of energies of interest to several physical chemical environments, where processes leading to fragment-ion production are important. A comprehensive comparison of the proton- and electron-impact data shows marked contrasts and similarities between both projectiles in the fragment-ion production. While NH_3^+ and NH_2^+ show similar yields for both projectiles above $v = 3$ a.u., the electron yields of all other fragment ions are larger than the proton yields, showing the effect of the charge sign in the ionization of the ammonia, previously observed for the methane molecule.

A semi-empirical model used to describe the ion fragment production showed that some fragments in the single ionization cannot be described solely by a picture where only a single hole vacancy mechanism occurs. Instead a two-step mechanism, ionization plus excitation, is needed to explain the change in the energy dependence towards lower energies for N^+ and NH^+ fragments. The vertical transition of single states forms the parent and NH_2^+ fragment ion, while shake-up and ionization-excitation two-step-two processes produces the NH^+, N^+, H^+, and H_2^+ fragment ions. The contribution of the ammonia molecular orbitals to the fragment production was evaluated by the semi-empirical fragmentation matrix model and compared with electron data. A reasonable agreement was found between the distinct approaches, fragmentation matrix model and dipole-breakdown picture. The fragmentation matrix model proved reliable to describe the NH_3^+ and NH_2^+ experimental cross section over the entire energy range and for NH^+, N^+, H^+, H_2^+ above 250 keV. It failed below that energy because the ionization-excitation two-step-two was not included.

The double ionization is dominated by the break-up of the double charged parent ion, but even so the parent dication survives under proton impact. The competitive two-step-two and nitrogen K-shell Auger-deexcitation processes are present in double ionization and triple ionization, and the latter process dominates at higher energies. The independent atom model-pixel counting method calculations describe well the single ionization, but it fails to describe the multiple ionization.

[1] V. N. Salinas, M. R. Hogerheijde, E. A. Bergin, L. I. Cleeves, C. Brinch, G. A. Blake, D. C. Lis, G. J. Melnick, O. Panić, J. C. Pearson, L. Kristensen, U. A. Yildiz, and E. F. van Dishoeck, First detection of gas-phase ammonia in a planet-forming disk. NH₃, N₂H⁺, and H₂O in the disk around TW Hydrae, Astron. Astrophys. **591**, A122 (2016).

[2] K. Altwegg, H. Balsiger, N. Hänni, M. Rubin, M. Schuhmann, I. Schroeder, T. Sémon, S. Wampfler, J.-J. Berthelier, C. Briois, M. Combi, T. I. Gombosi, H. Cottin, J. De Keyser, F. Dhooghe, B. Fiethe, and S. A. Fuselier, Evidence of ammonium salts in comet 67p as explanation for the nitrogen depletion in cometary comae, Nat. Astron. **4**, 533 (2020).

[3] S. Pizzarello and L. B. Williams, Ammonia in the early solar system: An account from carbonaceous meteorites, Astrophys. J. **749**, 161 (2012).

[4] P. C. Myers and P. J. Benson, Dense cores in dark clouds. II. NH₃ observations and star formation, Astrophys. J. **266**, 309 (1983).

[5] K. E. Mandt, O. Mousis, J. Lu-nine, and D. Gautier, Protosolar Ammonia as the Unique Source of Titan's Nitrogen, Astrophys. J. **788**, L24 (2014).

[6] C. M. Dalle Ore, D. P. Cruikshank, S. Protopapa, F. Scipioni, W. B. McKinnon, J. C. Cook, W. M. Grundy, B. Schmitt, S. A. Stern, J. M. Moore, A. Verbiscer, A. H. Parker, K. N. Singer,

O. M. Umurhan, H. A. Weaver, C. B. Olkin, L. A. Young, and K. Ennico, Detection of ammonia on Pluto's surface in a region of geologically recent tectonism, Sci. Adv. **5** (2019).

[7] K. M. Pontoppidan, C. Salyk, A. Banzatti, G. A. Blake, C. Walsh, J. H. Lacy, and M. J. Richter, The nitrogen carrier in inner protoplanetary disks, Astrophys. J. Lett. **874**, 92 (2019).

[8] E. M. Dunne, H. Gordon, A. Kürten, J. Almeida, J. Duplissy, C. Williamson, I. K. Ortega, K. J. Pringle, A. Adamov, U. Baltensperger, P. Barmet, F. Benduhn, F. Bianchi, M. Breitenlechner, A. Clarke, J. Curtius, J. Dommen, N. M. Donahue, S. Ehrhart, R. C. Flagan, *et al.*, Global atmospheric particle formation from CERN CLOUD measurements, Science **354**, 1119 (2016).

[9] M. Höpfner, R. Volkamer, U. Grabowski, M. Grutter, J. Orphal, G. Stiller, T. von Clarmann, and G. Wetzel, First detection of ammonia NH_3 in the Asian summer monsoon upper troposphere, Atmos. Chem. Phys. **16**, 14357 (2016).

[10] J. F. Kasting, Stability of ammonia in the primitive terrestrial atmosphere, J. Geophys. Res. **87**, 3091 (1982).

[11] L. Y. Stein and M. G. Klotz, The nitrogen cycle, Curr. Biol. **26**, R94 (2016).

[12] M. G. P. Homem, I. Iga, G. L. C. de Souza, A. I. Zanelato, L. E. Machado, J. R. Ferraz, A. S. dos Santos, L. M. Brescansin, R. R. Lucchese, and M.-T. Lee, Electron collisions with ammonia and formamide in the low- and intermediate-energy ranges, Phys. Rev. A **90**, 062704 (2014).

[13] B. Jochim, A. Lueking, L. Doshier, S. Carey, E. Wells, E. Parke, M. Leonard, K. D. Carnes, and I. Ben-Itzhak, Rapid formation of H_3^+ from ammonia and methane following 4 MeV proton impact, J. Phys. B: At., Mol. Opt. Phys. **42**, 091002 (2009).

[14] D. J. Lynch, L. H. Toburen, and W. E. Wilson, Electron emission from methane, ammonia, monomethylamine, and dimethylamine by 0.25 to 2.0 MeV protons, J. Chem. Phys. **64**, 2616 (1976).

[15] R. J. McNeal, Production of positive ions and electrons in collisions of 1–25-keV protons and hydrogen atoms with CO, CO_2, CH_4, and NH_3, J. Chem. Phys. **53**, 4308 (1970).

[16] M. E. Rudd, Y. K. Kim, D. H. Madison, and J. W. Gallagher, Electron production in proton collisions: Total cross sections, Rev. Mod. Phys. **57**, 965 (1985).

[17] M. V. V. S. Rao and S. K. Srivastava, Total and partial ionization cross sections of NH_3 by electron impact, J. Phys. B: At., Mol. Opt. Phys. **25**, 2175 (1992).

[18] K. Bederski, L. Wójcik, and B. Adamczyk, Ionization of ammonia by electron impact at 25–1000 eV, Int. J. Mass Spectrom. Ion Phys. **35**, 171 (1980).

[19] T. D. Märk, F. Egger, and M. Cheret, Ionization of ammonia and deuterated ammonia by electron impact from threshold up to 180 eV, J. Chem. Phys. **67**, 3795 (1977).

[20] A. Crowe and J. W. McConkey, Cross-sections for the direct and dissociative ionization of NH_3 by electron impact, Int. J. Mass Spectrom. Ion Phys. **24**, 181 (1977).

[21] R. Rejoub, B. G. Lindsay, and R. F. Stebbings, Electron-impact ionization of NH_3 and ND_3, J. Chem. Phys. **115**, 5053 (2001).

[22] E. C. Montenegro, G. M. Sigaud, and R. D. DuBois, Projectile and target scaling of the total ionization cross sections of atoms and molecules, Phys. Rev. A **87**, 012706 (2013).

[23] H. Luna, W. Wolff, E. C. Montenegro, and L. Sigaud, CH_4 fragmentation from single and double ionization by proton and electron impact, Phys. Rev. A **99**, 012709 (2019).

[24] W. Wolff, B. Rudek, L. A. da Silva, G. Hilgers, E. C. Montenegro, and M. G. P. Homem, Absolute ionization and dissociation cross sections of tetrahydrofuran: Fragmentation-ion production mechanisms, J. Chem. Phys. **151**, 064304 (2019).

[25] W. Wolff, H. Luna, and E. C. Montenegro, Isomeric signatures in the fragmentation of pyridazine and pyrimidine induced by fast ion impact, J. Chem. Phys. **143**, 044314 (2015).

[26] A. O. Bawagan, R. Müller-Fiedler, C. E. Brion, E. R. Davidson, and C. Boyle, The valence orbitals of NH_3 by electron momentum spectroscopy: Quantitative comparisons using Hartree-Fock limit and correlated wave functions, Chem. Phys. **120**, 335 (1988).

[27] M. Ishida, M. Ehara, and H. Nakatsuji, Outer- and inner-valence ionization spectra of NH_3, PH_3, and AsH_3: Symmetry-adapted cluster configuration interaction general-*R* study, J. Chem. Phys. **116**, 1934 (2002).

[28] L. Ishikawa, T. Odagiri, K. Yachi, T. Nakazato, M. Kurokawa, M. Kitajima, and N. Kouchi, Doubly excited states of ammonia produced by photon and electron interactions, J. Phys. B: At., Mol. Opt. Phys. **41**, 195204 (2008).

[29] G. R. Wight, M. J. V. der Wiel, and C. E. Brion, Dipole oscillator strengths for excitation, ionisation and fragmentation of NH_3 in the 5 to 60 eV region, J. Phys. B: At. Mol. Phys. **10**, 1863 (1977).

[30] C. E. Brion, A. Hamnett, G. R. Wight, and M. J. Van der Wiel, Branching ratios and partial oscillator strengths for the photoionization of NH_3 in the 15–50 eV region, J. Electron Spectrosc. Relat. Phenom. **12**, 323 (1977).

[31] S. P. Khare, S. Prakash, and W. J. Meath, Dissociative ionization of NH_3 and H_2O molecules by electron impact, Int. J. Mass Spectrom. Ion Processes **88**, 299 (1989).

[32] H. J. Lüdde, M. Horbatsch, and T. Kirchner, Proton-impact-induced electron emission from biologically relevant molecules studied with a screened independent atom model, J. Phys. B: At., Mol. Opt. Phys. **52**, 195203 (2019).

[33] A. C. Tavares, H. Luna, W. Wolff, and E. C. Montenegro, Double ionization of water molecules induced by swift protons, Phys. Rev. A **92**, 032714 (2015).

[34] H. Knudsen, U. Mikkelsen, K. Paludan, K. Kirsebom, S. P. Moller, E. Uggerhoj, J. Slevin, M. Charlton, and E. Morenzoni, Non-dissociative and dissociative ionization of N_2, CO, CO_2, and CH_4 by impact of 50–6000 keV protons and antiprotons, J. Phys. B: At., Mol. Opt. Phys. **28**, 3569 (1995).

[35] W. Wolff, I. J. de Souza, A. C. Tavares, G. F. S. de Oliveira, and H. Luna, Electron-recoilion and recoil ion-projectile coincidence techniques applied to obtain absolute partial collision cross section, Rev. Sci. Instrum **83**, 123107 (2012).

[36] I. Ben-Itzhak, S. G. Ginther, and K. D. Carnes, Multiple-electron removal and molecular fragmentation of CO by fast F^{4+} impact, Phys. Rev. A **47**, 2827 (1993).

[37] M. Simon, T. LeBrun, P. Morin, M. Lavollée, and J. L. Maréchal, A photoelectron-ion multiple coincidence technique applied to core ionization of molecules, Nucl. Instrum. Methods Phys. Res., Sect. B **62**, 167 (1991).

[38] R. Locht, J. L. Olivier, and J. Momigny, Dissociative autoionization as a mechanism for the proton formation from methane and methane-d4 by low energy electron impact, Chem. Phys. **43**, 425 (1979).

[39] R. Locht and J. Momigny, The proton formation from methane by dissociative ionization in the electron energy range of 25–40 eV, Chem. Phys. **49**, 173 (1980).

[40] R. Locht and J. Momigny, The dissociative electroionization of ammonia and ammonia-d3. III. the N^+ dissociation channel. general conclusions about the dissociation of NH_3^+, Chem. Phys. **127**, 435 (1988).

[41] R. Locht, Ch. Servais, M. Ligot, M. Davister, and J. Momigny, The dissociative electroionization of ammonia and ammonia-d3. II. The H^+ and H_2^+ dissociation channels, Chem. Phys. **125**, 425 (1988).

[42] R. Locht and J. Momigny, The double ionization of ammonia. Its dissociation into the doubly ionized fragment N^{2+}, Chem. Phys. Lett. **138**, 391 (1987).

[43] C. C. Montanari and J. E. Miraglia, Neonization method for stopping, mean excitation energy, straggling, and for total and differential ionization cross sections of CH_4, NH_3, H_2O and FH by impact of heavy projectiles, J. Phys. B: At. Mol. Opt. Phys. **47**, 015201 (2014).

[44] H. J. Lüdde (private communication).

[45] M. V. V. S. Rao and S. K. Srivastava, Cross sections for direct and dissociative ionization of NH_3 and CS_2 by electron impact, J. Geophys. Res. **96**, 17563 (1991).

[46] J. R. Hamilton, J. Tennyson, S. Huang, and M. J. Kushner, Calculated cross sections for electron collisions with NF_3, NF_2 and NF with applications to remote plasma sources, Plasma Sources Sci. Technol. **26**, 065010 (2017).

[47] Y.-K. Kim, W. Hwang, N. M. Weinberger, M. A. Ali, and M. E. Rudd, Electron-impact ionization cross sections of atmospheric molecules, J. Chem. Phys. **106**, 1026 (1997).

[48] W. Hwang, Y.-K. Kim, and M. E. Rudd, New model for electron-impact ionization cross sections of molecules, J. Chem. Phys. **104**, 2956 (1996).

[49] H. J. Lüdde, M. Horbatsch, and T. Kirchner, A screened independent atom model for the description of ion collisions from atomic and molecular clusters, Eur. Phys. J. B **91**, 99 (2018).

[50] D. K. Jain and S. P. Khare, Ionizing collisions of electrons with CO_2, CO, H_2O, CH_4 and NH_3, J. Phys. B: At. Mol. Phys. **9**, 1429 (1976).

[51] S. P. Khare and W. J. Meath, Cross sections for the direct and dissociative ionisation of NH_3, H_2O and H_2S by electron impact, J. Phys. B: At. Mol. Phys. **20**, 2101 (1987).

[52] V. Saksena, M. S. Kushwaha, and S. P. Khare, Ionization cross-sections of molecules due to electron impact, Phys. B (Amsterdam, Neth.) **233**, 201 (1997).

[53] H. Deutsch, K. Becker, S. Matt, and T. D. Märk, Theoretical determination of absolute electron-impact ionization cross sections of molecules, Int. J. Mass Spectrom. **197**, 37 (2000).

[54] J. A. Syage, Spectroscopy and dynamics of jet-cooled hydrazines and ammonia. II. Electron-impact dissociative ionization, J. Chem. Phys. **97**, 6085 (1992).

[55] V. Tarnovsky, H. Deutsch, and K. Becker, Cross-sections for the electron impact ionization of ND_x ($x = 1$–3), Int. J. Mass Spectrom. Ion Processes **167–168**, 69 (1997).

[56] R. Locht, Ch. Servais, M. Ligot, Fr. Derwa, and J. Momigny, The dissociative electroionization of ammonia and ammonia-d3. I. the NH^+ and NH_2^+ dissociation channels, Chem. Phys. **123**, 443 (1988).

[57] J. H. McGuire, Perturbation expansions, in *Electron Correlation Dynamics in Atomic Collisions*, Cambridge Monographs on Atomic, Molecular and Chemical Physics (Cambridge University Press, 1997), pp. 144–173. .

[58] J. H. McGuire, Double Ionization of Helium by Protons and Electrons at High Velocities, Phys. Rev. Lett. **49**, 1153 (1982).

[59] J. H. Mcguire, *Multiple-Electron Excitation, Ionization, and Transfer in High-Velocity Atomic and Molecular Collisions* (Academic Press, 1991) pp. 217–323.

[60] A. Salehzadeh and T. Kirchner, Fragmentation of methane molecules by proton and antiproton impact, Eur. Phys. J. D **71**, 66 (2017).

[61] T. Kirchner and H. Knudsen, Current status of antiproton impact ionization of atoms and molecules: Theoretical and experimental perspectives, J. Phys. B: At., Mol. Opt. Phys. **44**, 122001 (2011).

[62] O. G. de Lucio and R. D. DuBois, Differential studies and projectile charge effects in ionization of molecular nitrogen by positron and electron impact, Phys. Rev. A **93**, 032710 (2016).

[63] J. H. McGuire, Correlation in atomic scattering, Phys. Rev. A **36**, 1114 (1987).

[64] K. L. Nixon, A. J. Murray, H. Chaluvadi, C. Ning, J. Colgan, and D. H. Madison, Low energy (*e*, 2*e*) coincidence studies of NH_3: Results from experiment and theory, J. Chem. Phys. **138**, 174304 (2013).

[65] L. S. Cederbaum, W. Domcke, J. Schirmer, and W. V. Niessen, Correlation effects in the ionization of molecules: Breakdown of the molecular orbital picture, in *Advances in Chemical Physics* (John Wiley & Sons, Ltd., 2007), pp. 115–159. .

[66] F. H. Dorman and J. D. Morrison, Double and triple ionization in molecules induced by electron impact, J. Chem. Phys. **35**, 575 (1961).

[67] M. M. Mann, A. Hustrulid, and J. T. Tate, The ionization and dissociation of water vapor and ammonia by electron impact, Phys. Rev. **58**, 340 (1940).

[68] J. D. Morrison and J. C. Traeger, Ionization and dissociation by electron impact II. NH_3 and PH_3, Int. J. Mass Spectrom. Ion Phys. **11**, 277 (1973).

[69] E. C. Montenegro, L. Sigaud, W. Wolff, H. Luna, and Ferreira Natalia, Some dynamical features of molecular fragmentation by electrons and swift ions, Phys. Procedia **66**, 39 (2015).

[70] J. Appell and J. A. Horsley, Electronic states of doubly ionized ammonia, J. Chem. Phys. **60**, 3445 (1974).

[71] D. Winkoun and G. Dujardin, Fragmentation of doubly charged ammonia cations NH_3^{++} studied by the photoion-photoion coincidence (pipico) method, Z. Phys. D: At., Mol. Clusters **4**, 57 (1986).

[72] R. K. Boyd, S. Singh, and J. H. Beynon, Delayed predissociation and collision-induced processes of the ammonia di-cation NH_3^{2+}, Chem. Phys. **100**, 297 (1985).

[73] C. C. Montanari and J. E. Miraglia, Antiproton, proton and electron impact multiple ionization of rare gases, J. Phys. B: At. Mol. Opt. Phys. **45**, 105201 (2012).

[74] M. Batic, M. G. Pia, and S. J. Cipolla, Isicsoo: A class for the calculation of ionization cross sections from ECPSSR and PWBA theory, Comput. Phys. Commun. **183**, 398 (2012).